Dyes and Pigments 170 (2019) 107635

Contents lists available at ScienceDirect

Dyes and Pigments

journal homepage: www.elsevier.com/locate/dyepig

Octachloro-fluorescein: Synthesis and photosensitizer performance evaluation

Ying Wang, Hanjiao Chen, Chenghui Li, Peng Wu*

Analytical & Testing Center, Sichuan University, Chengdu, 610064, China

ARTICLE INFO

Keywords:
Photosensitizer
Singlet oxygen
Heavy atom effect
Image-guide PDT
Fluorescein

ABSTRACT

Fluorescence image-guided photodynamic therapy (PDT) receives great attention since it provides both the diagnostic and therapeutic information. Theoretically, fluorescence and the photodynamic performance (singlet oxygen) can be traced back to the same origin, namely the Jablonski energy diagram. Therefore, designing photosensitizers with balanced fluorescence and singlet oxygen generation is essentially important. Heavy atom effect (HAE) is an effective approach for designing highly efficient photosensitizers, but at the sacrifice of fluorescence. Herein, through analysis of the well-known fluorophore fluorescein and the photosensitizer Rose Bengal (RB), a new kind of photosensitizer, octachloro-fluorescein (OCF), was designed and synthesized. Structurally, OCF was obtained through anchoring chlorine atoms (heavier than H but lighter than I) onto all the existing open sites of fluorescein, resting in a 5-fold singlet oxygen quantum yield increase over fluorescein, but a much higher fluorescence quantum yield (Φ_{fl} = 0.628) over RB. The photodynamic performance of OCF was characterized both photophysically and photochemically. Besides, the image-guided PDT performance of OCF was further evaluated with HeLa cells, demonstrating that elegant heavy atom substitution of fluorescein may provide an effective way of balancing the fluorescence and singlet oxygen generation.

1. Introduction

Photosensitization or a photodynamic process refers to the light-induced reaction, in which light, photosensitizer, and oxygen are the three basic components [1,2]. During such a process (Scheme 1), the photosensitizer (PS) first absorbs light for excitation to the excited singlet state, followed by either emitting prompt fluorescence via decaying back to the ground state, or activating the triplet state through intersystem crossing (ISC). Upon interaction of oxygen with the triplet state, energy transfer from triplet state to ground state oxygen ($^3O_2$) occurs, leading to the generation of singlet oxygen ($^1O_2$). The highly active nature of singlet oxygen can be harvested for a variety of photosensitization or photodynamic applications, such as photodynamic antimicrobial chemotherapy (PACT) [3,4], and photoinduced organic synthesis [5]. Particularly, photodynamic therapy (PDT), relying on cell ablation by photosensitized generation of singlet oxygen, has been widely treatment of cancer [6–10] and other disease (e.g., Alzheimer's disease [11]). To increase the singlet oxygen generation, anchoring photosensitizers with heavy atoms, namely heavy atom effect (HAE), is an effective approach, which promotes spin-orbit coupling and thus increased ISC [12–14].

For modern cancer therapy, image-guided PDT receives great attention since it unites the diagnostic and therapeutic effect in a single agent, allowing for simultaneous diagnosis and treatment responses [15–17]. From the photophysical point of view, photosensitizers provides intrinsic chances for designing image-guided PDT. On one hand, the fluorescence from the photosensitizers allows sensitive imaging-based operations. On the other hand, singlet oxygen generated from photosensitization can be explored for effective therapy. Therefore, the key factor to achieve effective image-guided PDT is to design photosensitizers capable of simultaneous bright fluorescence and good singlet oxygen generation performance. Although heavy atom effect is effective in promoting singlet oxygen generation, it is at the sacrifice of fluorescence energy, namely quenching of fluorescence [18–21]. Therefore, designing photosensitizers with balanced fluorescence and singlet oxygen generation is essentially important for potential image-guided PDT.

Fluorescein (Scheme 1B), a classical xanthene dye with high fluorescence quantum yield and excellent water solubility, is well-known for its widespread use as fluorescent detection reagents and probes for bioimaging applications [22–24]. Some derivatives of fluorescein are also the most widely used fluorescent derivatization reagents in cytology and immunohistochemistry. Normally, the singlet oxygen quantum yield of fluorescein is typically very low (Φ_Δ = 0.03), which is

* Corresponding author.
E-mail address: wupeng@scu.edu.cn (P. Wu).

https://doi.org/10.1016/j.dyepig.2019.107635
Received 17 May 2019; Received in revised form 7 June 2019; Accepted 7 June 2019
Available online 11 June 2019
0143-7208/

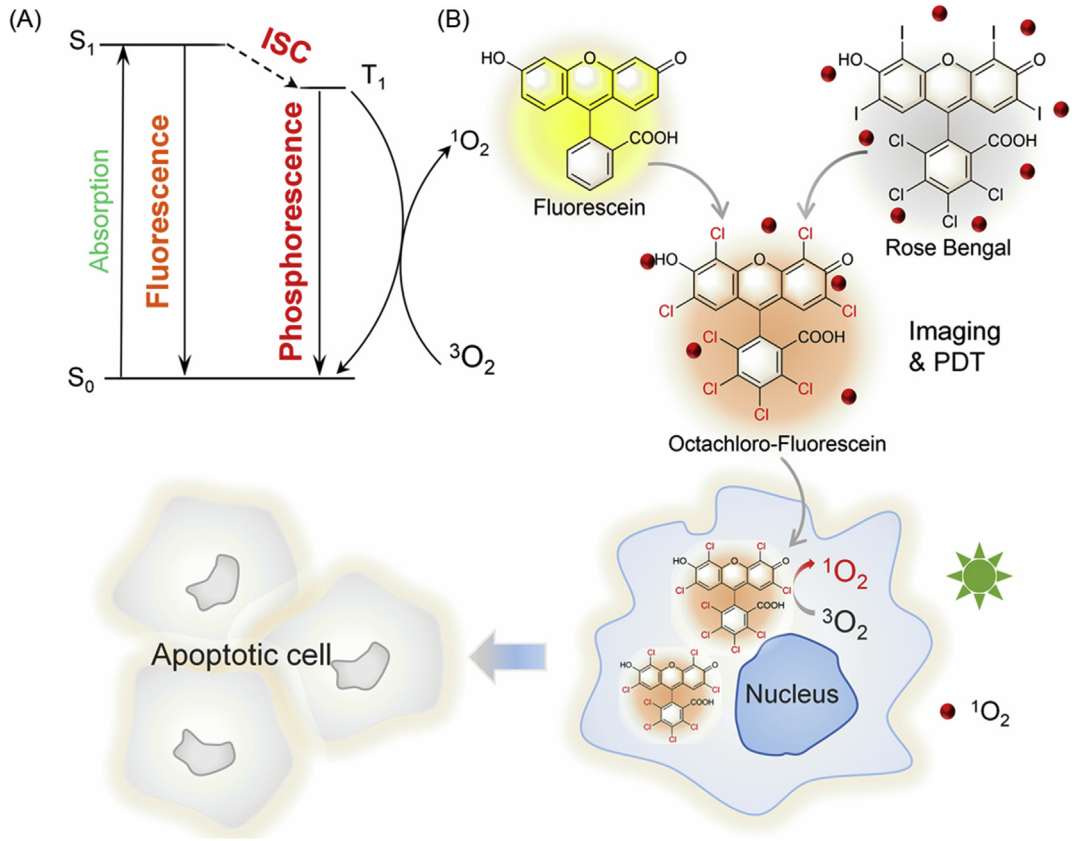

Scheme 1. Image-guided photodynamic cancer therapy of OCF.

not suitable for PDT applications. Heavy atom substituted fluorescein derivatives, such as tetrachlorotetraiodo-fluorescein (Rose Bengal, RB, Scheme 1B), are well-known photosensitizers for a variety of photodynamic applications [25]. Although featuring high singlet oxygen quantum yield (Φ_{Δ} = 0.75) [26], the fluorescence of RB (Φ_{fl} = 0.003) is largely lower than that of fluorescein (Φ_{fl} = 0.848), which limited its use in image-guided PDT.

Therefore in this work, we designed and synthesized a kind of photosensitizer through substituting the iodine atoms in RB with chlorine, namely 2′,4′,5′,7′-tetrachloro-4,5,6,7-tetrachlorofluorescein (OCF). The photosensitization performance of OCF was evaluated through detailed photophysical characterizations. By anchoring chlorine atoms onto the xanthene ring of fluorescein, OCF displayed a ~5-fold singlet oxygen quantum yield increase, but still possesses high fluorescence quantum yield (Φ_{fl} = 0.628). Besides, the image-guided PDT performance of OCF was further evaluated in vivo with HeLa cells, demonstrating that elegant heavy atom substitution of fluorescein may provide an effectively way of balancing the fluorescence and singlet oxygen generation performance of fluorescein.

2. Results and discussion

2.1. Synthesis of OCF

Halo-fluorescein can be easily introduced into the ring of fluorescein via one-step condensation reaction with resorcinol and phthalic anhydride [27]. The detailed synthetic route for the new compound OCF (compound 4) from 2,4-dichlororesorcinol (compound 3) and tetrachlorophthalic anhydride was given in Scheme 2. To prepare compound 3, 2,4-dihydroxybenzoic acid (compound 1) was taken as the precursor, followed by chlorination with HCl and H_2O_2 to yield 3,5-dichloro-2,4-dihydroxybenzoic acid (compound 2, Fig. S1). Subsequent elimination of the carboxyl group in *N*,*N*-dimethylaniline yielded 2,4-

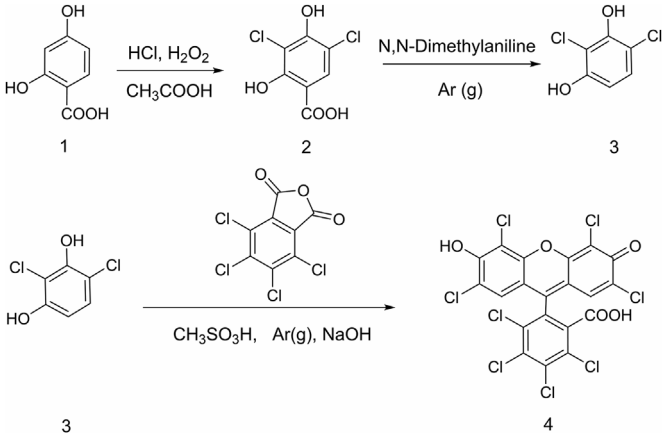

Scheme 2. Synthesis procedures for **OCF.**

dichlororesorcinol (compound 3, Fig. S2). Later, OCF (4) was obtained through condensation between 2,4-dichlororesorcinol (3) and tetrachlorophthalic anhydride, which was further characterized with ^{1}H NMR (Fig. S3), ^{13}C NMR (Fig. S4), MS (Fig. S5), and FT-IR (Fig. S6).

2.2. Photophysical characterizations

The photophysical properties of OCF, including the absorption, fluorescence, and phosphorescence spectra, were first collected. For conforming the heavy atom effect, the spectra of fluorescein and RB were also included. As shown in Fig. 1, the absorption and fluorescence spectra of these three compounds are generally similar in shape. The maximum absorption and fluorescence emission of fluorescein locate at 491 nm and 514 nm, respectively. Upon chlorination of fluorescein to

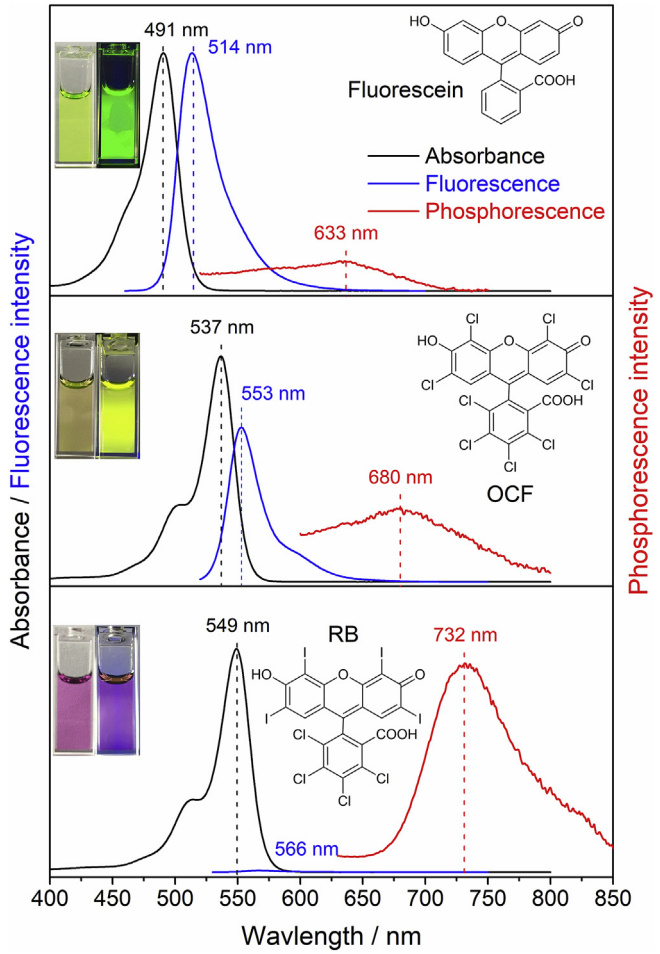

Fig. 1. The absorption, fluorescence and phosphorescence spectra of fluorescein, OCF, and RB (10 μM, H_2O, pH = 9).

yield OCF, red shift in both absorption (537 nm) and fluorescence emission (553 nm) occurred. For RB, the absorption and fluorescence were even red-shifted to 549 and 566 nm, respectively. For phosphorescence measurements, the above solutions were first degassed with nitrogen to remove dissolved oxygen, since phosphorescence is easily quenched by oxygen. After removal of oxygen, the phosphorescence emission (delay time of 50 μs) of fluorescein, OCF, and RB were observed at 633 nm, 680 nm, and 732 nm, respectively. Such spectra red shift is a clear sign of heavy atom effect together with the electron withdrawing effect of chloride and iodine [14,27].

Next, the fluorescence and phosphorescence emission of fluorescein, OCF, and RB were quantitatively compared. Generally, the apparent signature of heavy atom effect is simultaneous fluorescence quenching and phosphorescence enhancing [18]. As shown in Fig. 1, upon addition of chloride (OCF) and iodine (RB) to the skeleton of fluorescein, apparent fluorescence quenching was observed. Meanwhile, phosphorescence intensity of OCF was ~2-fold higher than fluorescein, but still lower than that of RB. The fluorescence quantum yield (Φ_{fl}) of OCF is 0.628 (Table 1, Fig. S8), which is only 1.35-fold lower than that of fluorescein (0.848), ensuring the potential cell imaging ability of OCF. But for RB, the Φ_{fl} is as low as ~0.003, barely suitable for cell imaging applications.

To further confirm the heavy atom effect, the fluorescence and phosphorescence decay behaviors of fluorescein, OCF, and RB (10 μM, H_2O) were compared. As shown in Fig. 2A, the fluorescence lifetime of OCF (4.15 ns) is shortened as compared with that of fluorescein (4.58 ns). While for RB, its fluorescence lifetime (~0.08 ns) is already close to the detection limit of our instrument. For phosphorescence

Table 1
Summary of the photophysical properties of fluorescein, OCF and RB (solvent: H_2O, pH = 9).

	Fluorescein	OCF	RB
Absorption (nm)	491	537	549
ε (10^4 M^{-1} cm^{-1})	9.95	5.49	8.57
Fluorescence (nm)	514	553	566
Stokes shift (nm)	23	16	17
τ_{fl} (ns)	4.58	4.15	0.08
Φ_{fl}	0.848	0.628	0.003
Phosphorescence (nm)	633	680	732
τ_{phos} (μs)	214.2	201.9	98.4
$k_{dec} \times 10^8$ (s^{-1})	2.18	2.41	125
$k_{rad} \times 10^8$ (s^{-1})	1.85	1.51	0.375
$k_{nr} \times 10^7$ (s^{-1})	3.31	8.97	124
Φ_Δ[a]	0.03	0.16	0.75

[a] For Φ_Δ evaluation, a mixed solvent of D_2O and CH_3CN (V_{D2O}: V_{CH3CN} = 1: 15) was used.

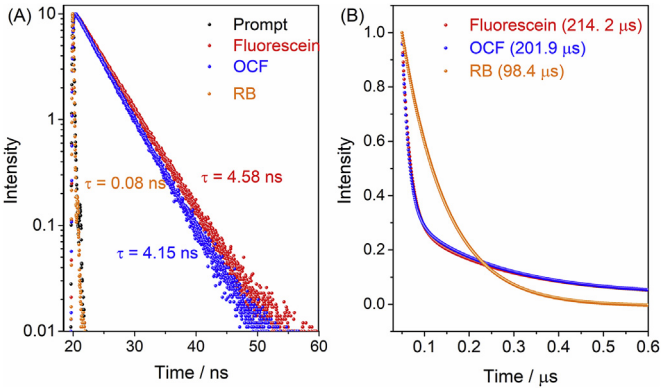

Fig. 2. Fluorescence (A) and phosphorescence (B) lifetime of fluorescein, OCF, and RB.

lifetime of fluorescein and OCF, it is difficult to be collected with the typical multichannel scanning technique due to the weak phosphorescence and strong interference from the fluorescence signal. Therefore, we employed the flash lamp for rough evaluation of the phosphorescence decay. As shown in Fig. 2B, the phosphorescence lifetime of OCF and RB (20 μM, H_2O) were also shortened as compared with that of fluorescein. The lifetime changes agreed well with the characteristics of heavy atom effect.

From the Jablonski energy diagram (Scheme 1A), it is known that the occurrence fluorescence and phosphorescence is typically accompanied by a series of non-radiative transitions. On the basis of the above photophysical parameters, the decay rate constants (k_{dec}), radiative rate constants (k_{rad}) and non-radiative rate constants (k_{nr}) of fluorescein, OCF and RB were calculated. As pointed out in Table 1, when fluorescein was substituted with heavy halogen atoms, about ~1-fold and ~57-fold drop in k_{dec} were obtained for OCF and RB, respectively. Meanwhile, the radiative rate constants were also decreased (fluorescein > OCF > RB), accompanied by increase in nonradiative rate constants. A 3-fold increase in k_{nr} of fluorescence after introduced Cl to the fluorescein core was recorded, indicating that besides the regular non-radiative transitions, ISC from excited singlet state to triplet state may occur. In order to get more formation about the excited triplet state, the nanosecond transient absorption (TA) spectra of fluorescein and OCF (20 μM) were collected in N_2-saturated solutions under the excitation of 532 nm laser. As shown in Fig. S9, the apparent TA signal OCF is stronger than that of fluorescein, which is in according with the above increased k_{nr} of fluorescence. For RB, even higher k_{nr} of fluorescence and stronger TA signal were obtained.

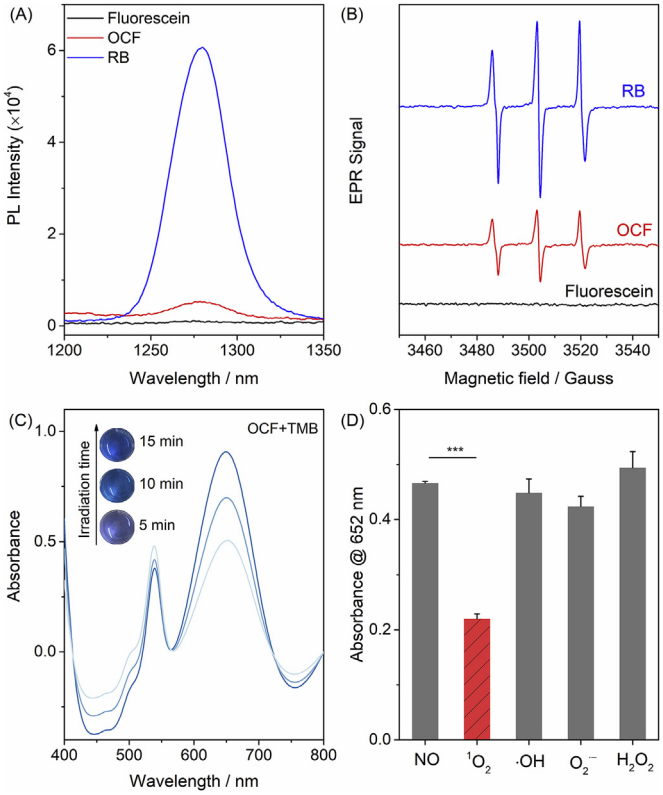

Fig. 3. Photochemical characterization of singlet oxygen: (A) phosphorescence emission spectra of singlet oxygen generated from photosensitization of fluorescein, OCF, and RB (10 μM, in the mixed solution, V_{D2O}: V_{CH3CN} = 1: 15); (B) EPR spectra singlet oxygen generated from photosensitization of fluorescein, OCF, and RB (10 μM, green LED, 2 min) in the presence of TEMP (a specific spin trap for $^1O_2$, final concentration is 100 mM); (C) time-dependent absorption spectra of TMB under LED (3 W) radiation in the presence of OCF (20 μM); and (D) identification of specific ROS generated from photosensitization of OCF with scavengers. (For interpretation of the references to color in this figure legend, the reader is referred to the Web version of this article.)

2.3. Photochemical characterizations

Molecule photosensitizers, typically working in type-II photosensitization, can produce highly active singlet oxygen for photodynamic applications. To monitor the photosensitized production of singlet oxygen, the characterized weak phosphorescence from decay of singlet oxygen [$^1O_2$ ($^1\Delta_g$) → O_2 ($^3\Sigma_g^-$)] is the most representative evidence. As shown in Fig. 3A, under the excitation at 536 nm, obvious singlet oxygen phosphorescence at ~1275 nm was collected from OCF and RB in a D_2O–CH_3CN mixed solvent (v/v = 1: 15), but not fluorescein. To further confirm such generation trend, electron paramagnetic resonance (EPR) was further explored for identification of the generated $^1O_2$, with 4-hydroxy-2,2,6,6-tetramethylpiperidine as the trapping agent. As shown in Fig. 3B, the EPR spectrum of OCF and RB displayed the characteristic peak of singlet oxygen, namely 1: 1: 1 typical triplet signal of 2,2,6,6-tetramethylpiperidine-noxyl (TEMPO). In agreement with the above phosphorescence characterization, there is also no appreciable EPR signal of singlet oxygen from fluorescein, confirming the low singlet oxygen quantum yield of fluorescein.

Next, the specific reactive oxygen species (ROS) generated form photosensitization of OCF was identified. First, we selected TMB (3,3′,5,5′-tetramethylbenzidine) as the substrate for characterization of the photosensitized oxidation capacity of OCF [28–30], which can be turned from colorless to blue upon oxidation. As shown in Fig. 3C, OCF could catalyze the oxidation TMB within 5 min under light emitting diode (LED) (λ = 520 nm, 3 W). The specific ROS responsible for TMB oxidation were identified with ROS-specific scavengers, namely tryptophan for $^1O_2$, mannitol for •OH, catalase for H_2O_2, and superoxide dismutase for $O_2^{\bullet-}$ [31–35]. As shown in Fig. 3D, only tryptophan could inhibit the TMB oxidation, indicating that singlet oxygen was the major ROS generated from photosensitization of OCF.

The singlet oxygen quantum yields (Φ_Δ) of fluorescein and OCF were evaluated with the $^1O_2$ phosphorescence emission integrated area with Rose Bengal (RB) as the standard photosensitizer (Φ_Δ = 0.75) (Figure S10 and Figure S11) [26]. As shown in Table 1, Φ_Δ of fluorescein and OCF were 0.03 and 0.16, respectively. Considering of the relatively high QY of both fluorescence (0.628) and singlet oxygen (0.16), OCF may be potentially useful for image-guided PDT applications.

2.4. Evaluation of the image-guide PDT performance of OCF

On the basis of the improved singlet oxygen generation from OCF (versus fluorescein), the PDT performance of OCF was first evaluated with HeLa cervical cancer cells as the target. For comparison, fluorescein and RB were also included. In cell culture media, slight red-shifted absorption and fluorescence emission of these photosensitizers were observed, accompanied by insignificant fluorescence quenching (Fig. S12). Next, the fluorescence imaging performance of OCF was evaluated. For such purpose, each dye was incubated with HeLa cells for 12 h and then the fluorescent signals were collected by confocal laser scanning microscope (CLSM). As show in Fig. 4, in the FITC channel, fluorescence from both fluorescein and OCF was observed, with higher signal from fluorescein-stained cells. While in the TRITC channel, higher fluorescence from OCF-stained cells over the fluorescein-stained ones was observed, probably because of the spectra red-shift. In addition, under laser irradiation (0.5 mW/cm^2) for 60 min, few fluorescence photo-bleaching was observed, demonstrating good photostability compared with fluorescein and RB (Fig. S13). Therefore, OCF can be both a fluorescent indicator and a singlet oxygen generator moiety, which is potentially useful for imaging-guided PDT. For RB-stained cells, no appreciable fluorescence was observed from neither the FITC nor the TRITC channel, indicating that RB may be solely functioned as a singlet oxygen generator.

The PDT performance of these photosensitizers was investigated with a standard Cell Counting Kit-8 (CCK-8) assay. As shown in Fig. 5A, after incubating HeLa cells with different concentrations of fluorescein/OCF/RB for 24 h, the cell viability were higher than 88%, demonstrating a good biocompatibility and low dark-toxicity of these dyes. Upon LED-irradiation (520 nm, 3 mW/cm^2) for 60 min, cell survival rates decreased in the order of RB > OCF > fluorescein (Fig. 5B), which is in good accordance with the singlet oxygen quantum yield of these dyes. Although the $^1O_2$ QY of OCF (Φ_Δ = 0.16) was lower than that of RB (Φ_Δ = 0.75), the half maximal inhibitory concentration (IC_{50}) of OCF (62.1 μM) was only 3.5-fold higher than that of RB (17.8 μM), implying good PDT performance.

The photo-toxicity of OCF was further confirmed by the live/dead cells staining with the Caclein-AM/propidium iodide (PI) kit. After staining, live and dead cells will exhibit green and red fluorescence, respectively. As shown in Fig. 5C, no red fluorescence can be seen from fluorescein-stained cells, while the green fluorescence decreased sharply in the order of fluorescein > OCF > RB, which agreed well with the above cell viability tests. Therefore, the PDT performance of OCF locates between those of fluorescein and RB.

3. Conclusion

In summary, a new kind of photosensitizer octachloro-fluorescein with balanced fluorescence and singlet oxygen generation, was designed and synthesized through substituting the open sites of fluorescein with eight chlorine atoms. Compared with fluorescein, OCF displayed a ~5-fold singlet oxygen quantum yield increase, due to the

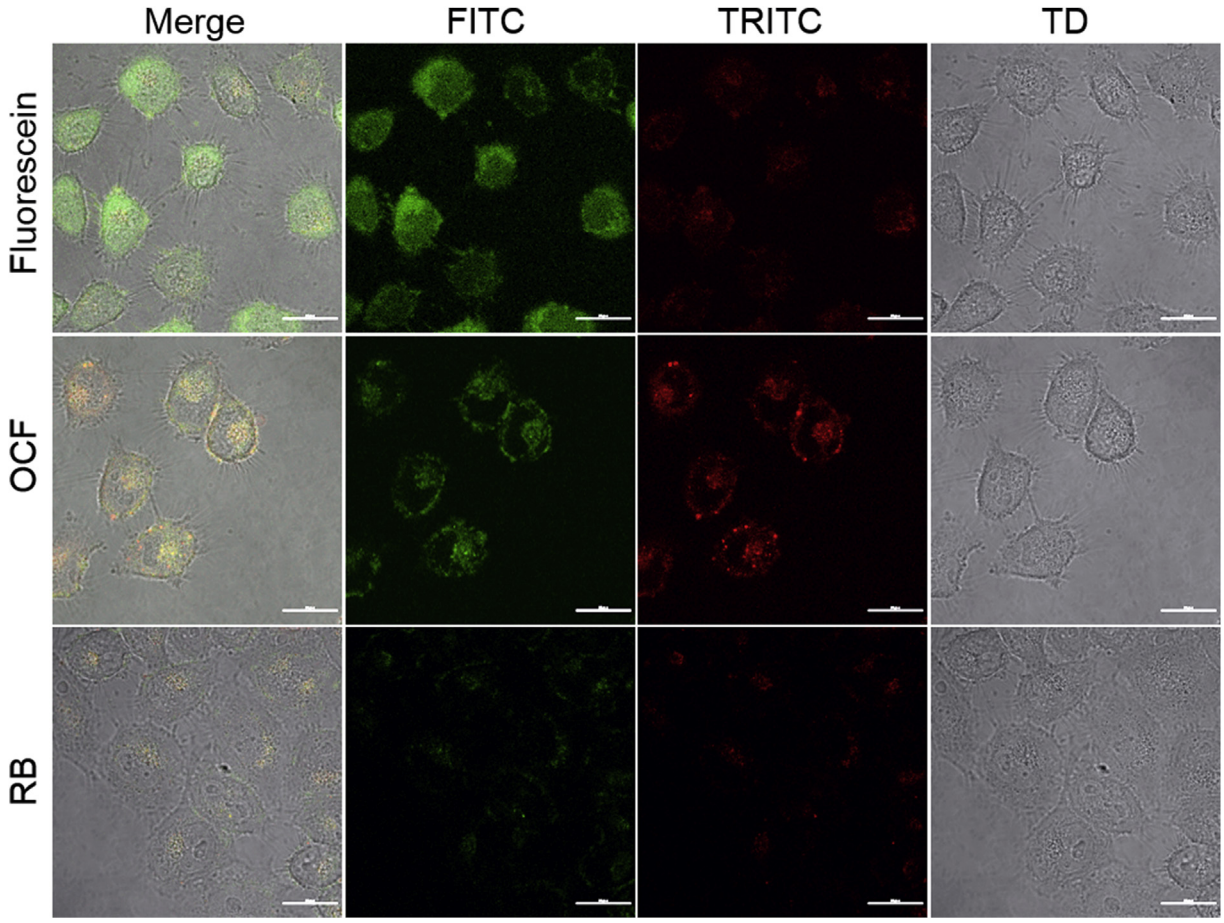

Fig. 4. The confocal images of HeLa cells with Fluorescein/OCF/RB-treated (c = 50 μM). The scale bar represent 20 μm.

introduction of heavier chlorine atoms. However, OCF possessed much higher fluorescence quantum yield (Φ_{fl} = 0.628) over RB, a structural analogue and an existing well-known photosensitizer. The potential image-guided PDT performance of OCF was evaluated in vivo with HeLa cells, which exhibited higher cell killing rates over fluorescein and brighter fluorescence over RB. Overall, the present study demonstrated that balanced fluorescence and singlet oxygen generation is essential for image-guided PDT, while careful heavy atom substitution of the existing fluorophores provides an elegant approach. Considering the existing versatile chemistry of facile functionalization of the fluorescein backbone, it is thus expected to further endow selective recognition of tumor cells of fluorescein-based photosensitizers for targeted imaging-guided PDT.

4. Experimental section

4.1. Chemical synthesis [27,36]

3,5-dichloro-2,4-dihydroxybenzoic acid (2): 2,4-dihydroxybenzoic acid **1** (32.4 mmol) and HCl (c, 194.6 mmol) were dissolved in CH_3COOH (10 ml) and 10 ml 30% H_2O_2 was added through the dropping funnel within 1 h. The mixed solution was stirred at 65 °C for 2 h and then cooled down to 4 °C. The precipitation was filtrated and washed with cold water, followed by recrystallization (v(H_2O): v(CH_3CH_2OH) = 2:1) to obtain 3,5-dichloro-2,4-dihydroxybenzoic acid **2** as white solid. ^{1}H NMR (400 MHz, DMSO): δ 7.66(1H Ar–H).

2,4-dichlororesorcinol **(3)**: a mixed solution containing **2** (8.97 mmol) and *N*,*N*-dimethylaniline (52.82 mmol) was heated to 190 °C for 0.5 h under stirring in the presence of Ar (g). Then, the reaction mixture was cooled down to room temperature, followed by addition of 7 mL concentrated HCl. The resultant mixture was extracted with ether for 5–6 times, the organic phase of which was washed with 6 M HCl and dried with anhydrous $MgSO_4$. Solvent was removed through vacuum-rotary evaporation to get the light blue solid. The solid was recrystallization by carbon tetrachloride to obtain white solid **3**.^{1}H NMR ($CDCl_3$, 400 MHz), δ 5.56 (1H, Ar-OH); 5.84 (1H, Ar-OH); 6.60–6.62 (2H, 6-ArH); 7.14–7.16 (2H, 5-ArH).

2′,4′,5′,7′-tetrachloro-4,5,6,7-tetrachlorofluorescein **(4)**: compound **3** (5.25 mmol) and tetrachlorophthalic anhydride (2.48 mmol) were dissolved in methanesulfonic acid and heated to 150 °C under Ar(g). Then, the reaction mixture was poured into ice-water (0 °C), followed by filtration and washing with ice-water to collect the solid. The dark pink solid was purified by silica gel chromatograph to get the target compound **4.**

2′,4′,5′,7′-tetrachloro-4,5,6,7-tetrachlorofluorescein (**4**): Yield 53%, MS (ESI): M + 1: 606.7424, ^{1}H NMR (DMSO, 400 MHz), δ: 11.21 (s, 2H, Ar-OH); 7.46 (s, 2H, Ar–H). ^{13}C NMR (101 MHz, DMSO) δ: 163.49, 152.44, 146.90, 146.59, 139.21, 135.84, 131.81, 127.30, 126.69, 125.22, 118.90, 110.40, 109.27. IR (KBr), ν, cm^{-1}: 3498, 2362, 1778, 1598, 1475, 1435, 1381, 1215, 1138, 999, 879, 813, 737.

4.2. Calculation of rate constants

The decay rate constants (k_{dec}), radiative rate constants (k_{rad}) and non-radiative rate constants (k_{nr}) of photosensitizers were calculated according to the following equations [37]:

$$k_{dec} = 1/\tau_{fl} \quad (1)$$

$$k_{rad} = \Phi_{fl}\, k_{dec} \quad (2)$$

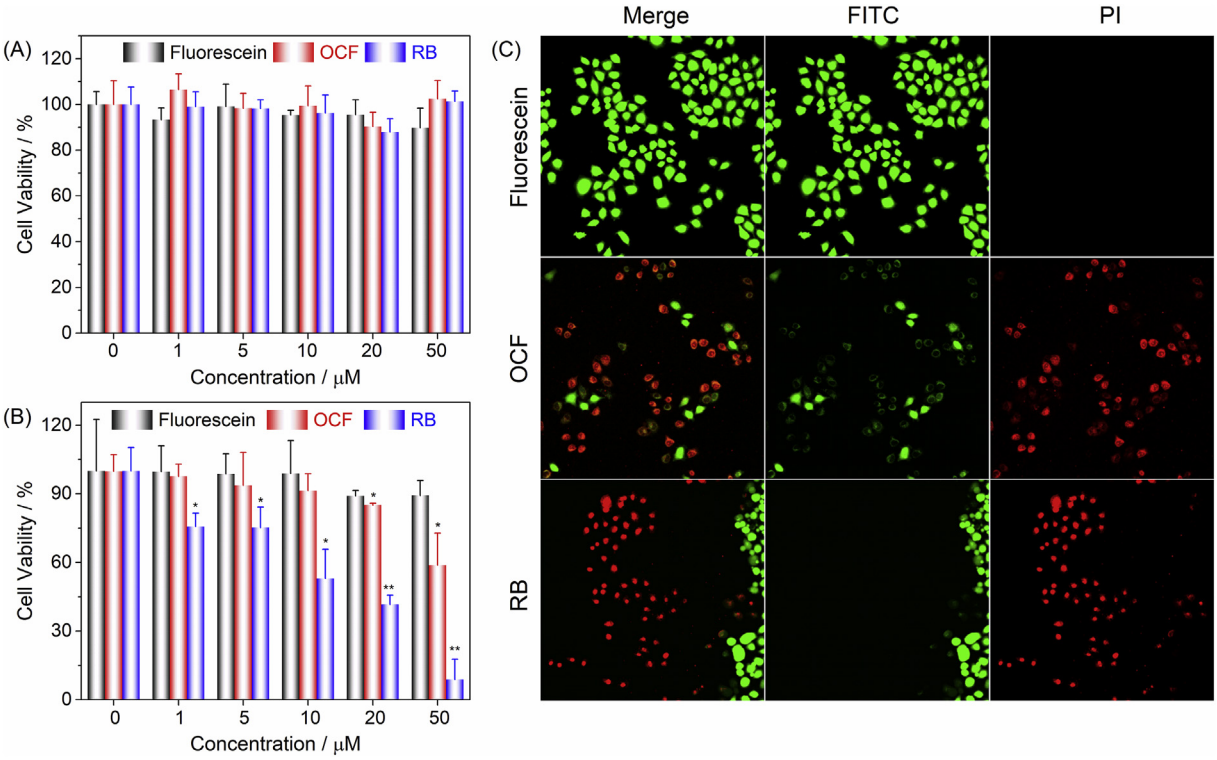

Fig. 5. The effect of PDT. (A) Live/Dead cells staining of Fluorescein/OCF/RB-treated HeLa cells. The concentration of photosensitizers were 50 μM. In all images, scale bars represent 50 μm; (B) the biocompatibility of Fluorescein/OCF/RB; and (C) the cell viability of different concentration fluorescein/OCF/RB-treated HeLa cells under LED-irradiated (520 nm, 3 mW/cm^2). *p < 0.05, **p < 0.01.

$$k_{nr} = (1 - \Phi_{fl})\, k_{dec} \quad (3)$$

4.3. Measurement of $^1O_2$ quantum yield

The singlet oxygen quantum yield was evaluated using RB as a standard ($\Phi_\Delta = 0.75$) [26]. The peak of the integrated absorption and $^1O_2$ phosphorescence emission of fluorescein, OCF and RB (10 μM) in mixed solvent (CH_3CN: D_2O = 15: 1) were collected by the CCD (Synapse) and NIR detector (Hamamatsu H-10330) of the fluorophotometer, respectively. The singlet oxygen quantum yield was calculated as follows:

$$\phi_{\triangle,Sample} = \frac{A_{1O_2,Sample}}{A_{absorbance,Sample}} \times \frac{A_{absorbance,\ RB}}{A_{1O_2,\ RB}} \times \phi_{\triangle,RB}$$

Here, $A_{1O2,\ sample}$ and $A_{1O2,\ RB}$ represent the integrated area of the $^1O_2$ phosphorescence emission of fluorescein/OCF and RB, $A_{absorbance,\ sample}$ and $A_{absorbance,\ RB}$ the Rayleigh scattering spectra area of fluorescein/OCF and RB respectively; $\Phi_{\Delta\ (RB)}$ is the $^1O_2$ quantum yield of RB.

4.4. Cell imaging

HeLa cells were cultured in glass culture dishes at a density of 10^5 cells/mL for 24 h. Fluorescein, OCF and RB (50 μM) were added into the culture medium (DMEM) and incubated with HeLa cells for 12 h (37 °C and 5% CO_2). The fluorescent images were taken with CLSM upon excitation at 488 nm and signal collection from 505 nm to 570 nm.

4.5. Cell viability test

HeLa cells were seeded in a 96-well plate at the density of 10^5 cells/mL and 100 μL per well for 24 h (37 °C and 5% CO_2). Different concentrations of fluorescein, OCF and RB were added into the medium and incubated with cells for another 12 h (37 °C and 5% CO_2). After subjected to light radiation (LED: 3 mW/cm^2, Ex 520 nm) for 60 min, the medium was removed and washed with phosphate-buffered saline (PBS) three times. Then, Cell Counting Kit-8 (CCK-8, 10 μL, 1 mg/mL) was added into the above 96-well plate for 1 h (37 °C and 5% CO_2). The absorbance at 450 nm was measured by microplate spectrophotometer. Cell survival rates were calculated through the ratio between absorbance of blank and samples.

4.6. Cell apoptosis analysis

HeLa cells were cultured in glass culture dishes for 24 h (37 °C and 5% CO_2). Fluorescein, OCF and RB (50 μM) were added into the cell culture medium and incubated with HeLa cells for 12 h. After light radiation (LED: 3 mW/cm^2, 520 nm) for 60 min, the cells were washed and incubated with Calcein-AM (cell-permeant dye, final concentration of 2 μM) and PI (Propidium Iodide, final concentration of 4 μM) for 15 min. The corresponding fluorescent images were taken by CLSM.

Acknowledgements

We gratefully acknowledge the financial support from the National Natural Science Foundation of China (No. 21522505), the Youth Science Foundation of Sichuan Province (Grant 2016JQ0019), and the Fundamental Research Funds for the Central Universities (2018SCUH0075).

Appendix A. Supplementary data

Supplementary data to this article can be found online at https://doi.org/10.1016/j.dyepig.2019.107635.

References

[1] Ogilby PR. Singlet oxygen: there is indeed something new under the sun. Chem Soc Rev 2010;39:3181–209.
[2] Schmidt R. Photosensitized generation of singlet oxygen. Photochem Photobiol 2006;82:1161–77.
[3] Hamblin MR, Hasan T. Photodynamic therapy: a new antimicrobial approach to infectious disease? Photochem Photobiol Sci 2004;3:436–50.
[4] Zhang YM, Zhao XW, Li YY, Wang X, Wang QS, Lu HG, Zhu LJ. A fluorescent photosensitizer with far red/near-infrared aggregation-induced emission for imaging and photodynamic killing of bacteria. Dyes Pigments 2019;165:53–7.
[5] Margaros I, Montagnon T, Tofi M, Pavlakos E, Vassilikogiannakis G. The power of singlet oxygen chemistry in biomimetic syntheses. Tetrahedron 2006;62:5308–17.
[6] Zhang X, Meng Z, Ma Z, Liu J, Han G, Ma F, Jia N, Miao Z, Zhang W, Sheng C, Yao J. Design and synthesis of novel water-soluble amino acid derivatives of chlorin p6 ethers as photosensitizer. Chin Chem Lett 2019;30:247–9.
[7] Wang C, Zhang Q, Wang X, Chang H, Zhang S, Tang Y, Xu J, Qi R, Cheng Y. Dynamic modulation of enzyme activity by near-infrared light. Angew Chem Int Ed 2017;56:6767–72.
[8] Jiang K, Wang YH, Cai CZ, Lin HW. Activating room temperature long afterglow of carbon dots via covalent fixation. Chem Mater 2017;29:4866–73.
[9] Lan M, Guo L, Zhao S, Zhang Z, Jia Q, Yan L, Xia J, Zhang H, Wang P, Zhang W. Carbon dots as multifunctional phototheranostic agents for photoacoustic/fluorescence imaging and photothermal/photodynamic synergistic cancer therapy. Adv Therap 2018;1:1800077.
[10] Lan M, Zhao S, Liu W, Lee C-S, Zhang W, Wang P. Photosensitizers for photodynamic therapy. Adv Healthc Mater 2019:1900132.
[11] Kuk S, Lee BI, Lee JS, Park CB. Rattle-structured upconversion nanoparticles for near-IR-induced suppression of alzheimer's β-amyloid aggregation. Small 2017;13:1603139.
[12] Zhao J, Xu K, Yang W, Wang Z, Zhong F. The triplet excited state of Bodipy: formation, modulation and application. Chem Soc Rev 2015;44:8904–39.
[13] Lim SH, Thivierge C, Nowak-Sliwinska P, Han J, van den Bergh H, Wagnières G, Burgess K, Lee HB. In vitro and in vivo photocytotoxicity of boron dipyrromethene derivatives for photodynamic therapy. J Med Chem 2010;53:2865–74.
[14] Durantini AM, Greene LE, Lincoln R, Martínez SR, Cosa G. Reactive oxygen species mediated activation of a dormant singlet oxygen photosensitizer: from autocatalytic singlet oxygen amplification to chemicontrolled photodynamic therapy. J Am Chem Soc 2016;138:1215–25.
[15] Ruan Z, Miao W, Yuan P, Le L, Jiao LJ, Hao EH, Yan LF. High singlet oxygen yield photosensitizer based polypeptide nanoparticles for low-power near-infrared light imaging-guided photodynamic therapy. Bioconjug Chem 2018;29:3441–51.
[16] Yuan YY, Zhang CJ, Gao M, Zhang RY, Tang BZ, Liu B. Specific light-up bioprobe with aggregation-induced emission and activatable photoactivity for the targeted and image-guided photodynamic ablation of cancer cells. Angew Chem Int Ed 2015;54:1780–6.
[17] Wang RG, Zhao MY, Deng D, Ye X, Zhang F, Chen H, Kong JL. An intelligent and biocompatible photosensitizer conjugated silicon quantum dots-MnO2 nanosystem for fluorescence imaging-guided efficient photodynamic therapy. J Mater Chem B 2018;6:4592–601.
[18] Koziar JC, Cowan DO. Photochemical heavy-atom effects. Acc Chem Res 1978;11:334–41.
[19] Hirayama T, Mukaimine A, Nishigaki K, Tsuboi H, Hirosawa S, Okuda K, Ebihara M, Nagasawa H. Bismuth-rhodamine: a new red light-excitable photosensitizer. Dalton Trans 2017;46:15991–5.
[20] Chiba M, Ichikawa Y, Kamiya M, Komatsu T, Ueno T, Hanaoka K, Nagano T, Lange N, Urano Y. An activatable photosensitizer targeted to gamma-glutamyltranspeptidase. Angew Chem Int Ed 2017;56:10418–22.
[21] Piao W, Hanaoka K, Fujisawa T, Takeuchi S, Komatsu T, Ueno T, Terai T, Tahara T, Nagano T, Urano Y. Development of an azo-based photosensitizer activated under mild hypoxia for photodynamic therapy. J Am Chem Soc 2017;139:13713–9.
[22] Gonçalves MST. Fluorescent labeling of biomolecules with organic probes. Chem Rev 2009;109:190–212.
[23] Chen X, Pradhan T, Wang F, Kim JS, Yoon J. Fluorescent chemosensors based on spiroring-opening of xanthenes and related derivatives. Chem Rev 2012;112:1910–56.
[24] Jin X, Hao L, Hu Y, She M, Shi Y, Obst M, Li J, Shi Z. Two novel fluorescein-based fluorescent probes for hypochlorite and its real applications in tap water and biological imaging. Sens Actuators B 2013;186:56–60.
[25] Abrahamse H, Hamblin Michael R. New photosensitizers for photodynamic therapy. Biochem J 2016;473:347–64.
[26] Redmond RW, Gamlin JN. A compilation of singlet oxygen yields from biologically relevant molecules. Photochem Photobiol 1999;70:391–475.
[27] Sun W-C, Gee KR, Klaubert DH, Haugland RP. Synthesis of fluorinated fluoresceins. J Org Chem 1997;62:6469–75.
[28] Zhang X, Deng L, Huang C, Zhang J, Hou X, Wu P, Liu J. Photosensitization of molecular oxygen on graphene oxide for ultrasensitive signal amplification. Chem Eur J 2018;24:2602–8.
[29] Zhang JY, Lu XM, Tang DD, Wu SH, Hou XD, Liu JW, Wu P. Phosphorescent carbon dots for highly efficient oxygen photosensitization and as photooxidative nanozymes. ACS Appl Mater Interfaces 2018;10:40808–14.
[30] Zhang JY, Wu SH, Lu XM, Wu P, Liu JW. Manganese as a catalytic mediator for photo-oxidation and breaking the pH limitation of nanozymes. Nano Lett 2019;19:3214–20.
[31] Li CB, Wang Y, Li CH, Xu SX, Hou XD, Wu P. Simultaneously broadened visible light absorption and boosted intersystem crossing in platinum-doped graphite carbon nitride for enhanced photosensitization. ACS Appl Mater Interfaces 2019. https://doi.org/10.1021/acsami.9b02767.
[32] Ju EG, Dong K, Chen ZW, Liu Z, Liu CQ, Huang YY, Wang ZZ, Pu F, Ren JS, Qu XG. Copper(II)-Graphitic carbon nitride triggered synergy: improved ROS generation and reduced glutathione levels for enhanced photodynamic therapy. Angew Chem Int Ed 2016;55:11467–71.
[33] Josephy PD, Eling T, Mason RP. The horseradish peroxidase-catalyzed oxidation of 3,5,3',5'-tetramethylbenzidine. Free radical and charge-transfer complex intermediates. J Biol Chem 1982;257:3669–75.
[34] Kellogg EW, Fridovich I. Superoxide, hydrogen peroxide, and singlet oxygen in lipid peroxidation by a xanthine oxidase system. J Biol Chem 1975;250:8812–7.
[35] Li CB, Xu Q, Xu SX, Zhang XF, Hou XD, Wu P. Synergy of adsorption and photosensitization of graphene oxide for improved removal of organic pollutants. RSC Adv 2017;7:16204–9.
[36] Chen ZT, Duan HF, Qiao S, Zhou WX, Qiu HW, Kang L, Xie XS, Huang YY. Fluorogenic sequencing using halogen-fluorescein-labeled nucleotides. ChemBioChem 2015;16:1153–7.
[37] Tian S, Ma H, Wang X, Lv A, Shi H, Geng Y, Li J, Liang F, Su Z-M, An Z, Huang W. Utilizing d–pπ bonds for ultralong organic phosphorescence. Angew Chem Int Ed 2019;58:6645–9.